AIP | Applied Physics Letters

Tunable topological electronic structures in Sb(111) bilayers: A first-principles study

Feng-Chuan Chuang, Chia-Hsiu Hsu, Chia-Yu Chen, Zhi-Quan Huang, Vidvuds Ozolins et al.

Citation: Appl. Phys. Lett. **102**, 022424 (2013); doi: 10.1063/1.4776734
View online: http://dx.doi.org/10.1063/1.4776734
View Table of Contents: http://apl.aip.org/resource/1/APPLAB/v102/i2
Published by the AIP Publishing LLC.

Tunable topological electronic structures in Sb(111) bilayers: A first-principles study

Feng-Chuan Chuang,[1,a)] Chia-Hsiu Hsu,[1] Chia-Yu Chen,[1] Zhi-Quan Huang,[1] Vidvuds Ozolins,[2] Hsin Lin,[3,a)] and Arun Bansil[3]
[1]*Department of Physics, National Sun Yat-Sen University, Kaohsiung 804, Taiwan*
[2]*Department of Materials Science and Engineering, University of California, Los Angeles, California 90095-1595, USA*
[3]*Department of Physics, Northeastern University, Boston, Massachusetts 02115, USA*

(Received 17 October 2012; accepted 3 January 2013; published online 18 January 2013)

Electronic structures and band topology of a single Sb(111) bilayer in the buckled honeycomb configuration are investigated using first-principles calculations. A nontrivial topological insulating phase can be induced by tensile strain, indicating the possibility of realizing the quantum spin Hall state for Sb thin films on suitable substrates. The presence of buckling provides an advantage in controlling the band gap through an out-of-plane external electric field, making a topological phase transition with six spin-polarized Dirac cones at the critical point. With a tunable gap and reversible spin polarization, Sb thin films are promising candidates for spintronic applications.
 [http://dx.doi.org/10.1063/1.4776734]

Recent theoretical prediction of topological insulators (TI) with nontrivial Z_2 topological invariant has rapidly gained attention.[1–4] The two dimensional (2D) TI, also known as the quantum spin Hall (QSH) phase, is a nonmagnetic insulator which harbors gapless edge states. These edge states lead to two spin-polarized currents propagating in opposite directions. A key feature of these gapless edge states is the absence of backscattering in the presence of nonmagnetic impurities and scatterers.[5,6] The three dimensional (3D) TI has been realized in a number of systems. These include the family of compounds based on bismuth (Bi) and antimony (Sb), such as $Bi_{(1-x)}Sb_x$,[7] Bi_2Se_3,[8–10] Bi_2Te_3,[8,11,12] and Sb_2Te_3.[12] As for 2D QSH systems, the first and most famous is graphene, but the gap in graphene is experimentally inaccessible.[4] The HgTe/CdTe quantum well has been theoretically proposed[14] and then experimentally shown to be in the 2D QSH state.[15,16] Theoretical studies have shown that the 2D QSH phase could be realized by reducing the dimensionality of 3D TIs in thin films. The band topology of these thin films is commonly perceived to depend sensitively on the film thickness, as shown for Bi_2Se_3 and Bi_2Te_3 ultrathin films.[19,20] The search for 2D QSH phases has been extended to Bi and Sb single-element materials since they have strong spin-orbit interactions. Murakami predicted a single Bi(111) bilayer (BL) film to be an elemental 2D TI.[17,18] Very recently, thin films of these two elements have been the subject of studies of quantum spin hall effect and topological insulators.[21–23] Ultrathin Bi(111) films have been characterized by a nontrivial Z_2 topological invariant for a wide range of film thicknesses,[21] whereas Sb(111) films with less than four Sb BLs are predicted to be topologically trivial.[23] It is not clear how to turn the Sb films into the QSH insulating state, and the topological properties of the electronic band structures under an out-of-plane external field have not been carefully explored.

In this work, atomic configurations as well as electronic band structures of Sb(111) single bilayers are investigated using first-principles calculations with the inclusion of spin-orbit coupling (SOC). The single bilayer structure can be regarded as a buckled honeycomb where the buckling can be reduced by the application of tensile strain in the in-plane direction. We find that at a critical value of tensile strain the buckled honeycomb bilayer transforms into a planar honeycomb structure. Within the strain range where the bilayer remains buckled, band inversion at the Brillouin zone center occurs at 4.6% tensile strain, causing a topological phase transition from a trivial band insulator with $Z_2 = 0$ to a nontrivial QSH insulator with $Z_2 = 1$. Moreover, we find that the planar Sb honeycomb sheet is a trivial insulator with $Z_2 = 0$. In the QSH phase, the presence of buckling provides an advantage in manipulating the spin-orbit band gap via adjusting the out-of-plane external electric field (gating). The external field not only induces an unbalanced charge distribution among the two Sb atoms but also breaks the inversion symmetry and lifts the spin degeneracy. A gating controlled topological phase transition is demonstrated by monitoring the band gap size as a function of the strength of the external field. At the topological critical point, conduction and valence bands meet each other at a point along the $\overline{\Gamma K}$ direction, forming six spin-polarized Dirac cones. The spin directions of the spin-split states as well as the spin helicities of the Dirac cones can be flipped by reversing the direction of the external field. Owing to the tunability of the polarization and the size of the band gap, Sb thin films possesses excellent potential for spintronic applications.

The calculations were carried out within the local density approximation (LDA) to the density-functional theory (DFT)[24–26] using the projector-augmented-wave (PAW) method[27] as implemented in the highly efficient Vienna *ab-initio* simulation package (VASP).[28] The kinetic energy cutoff was set to 172.3 eV and atomic positions were relaxed until the residual forces were less than 10^{-3} eV/Å. SOC was included in the band structure calculations using complex

[a)]Authors to whom correspondence should be addressed. Electronic addresses: fchuang@mail.nsysu.edu.tw and nilnish@gmail.com.

spinor wave functions and the second variational method. To model the single bilayer, a vacuum of ~12 Å was included in the supercell so that interactions between the two thin films in the periodic cell can be neglected. For bulk calculations, the Brillouin zone was sampled on a regular $21 \times 21 \times 21$ Monkhorst-Pack grid,[29] while $21 \times 21 \times 1$ Monkhorst-Pack grids were used to sample the 2D Brillouin zones of bilayer structures.

The thinnest Sb(111) film is the single bilayer structure shown in Fig. 1(a) which can be regarded as a buckled honeycomb. The bulk crystal structure of Sb is rhombohedral with two atoms in the primitive cell and can be described as a stacking of these bilayers along the [111] direction. In terms of the hexagonal lattice, the total-energy optimized lattice constants of bulk Sb are $a_0 = 4.29$ Å and $c_0 = 10.94$ Å, values that agree well with a previous study.[13] The equilibrium lattice constant, a, of the optimized Sb single bilayer is found to be 4.01 Å, which is 6.5% shorter than that of the calculated equilibrium bulk lattice constant, and the vertical distance between the two layers is found to be $d_1 = 1.64$ Å. The bilayer structure becomes a planar honeycomb ($d_1 = 0$) when the lattice constant a is increased to approximately 5 Å. The total energy as a function of strain (defined with respect to the bulk lattice constant a_0) is shown in Fig. 1(c). The solid line with filled squares shows the results obtained when the bilayer structure was gradually subjected to the applied tensile strain and the atoms were allowed to relax. The vertical distance between the bilayers as a function of the applied strain is shown in Fig. 1(c) as red crosses referring to the right axis. It shows that the buckled bilayer spontaneously transforms into the planar honeycomb structure at around $a = 5$ Å. In addition, we show by the results obtained when strain is gradually applied to the planar honeycomb structure [marked by asterisks in Fig. 1(c)] and the atoms are allowed to relax. The lattice constant of the optimized planar honeycomb structure is 4.9 Å and it is locally stable down to 4.6 Å, at which point it spontaneously buckles and transforms into the bilayer.

In what follows, we examine the band structure of the buckled Sb bilayer at different strain values. The band structures plotted in Figs. 2(a)–2(d) demonstrate our key findings. First, we focus on the band gaps at the Γ point. Figure 2(a) shows that an unstrained Sb bilayer exhibits a direct band gap of 0.75 eV at the Γ-point. The band gap at Γ as a function of strain is plotted in Fig. 2(h), which shows that the system undergoes a gap closing and reopening process. The band topology is investigated by identifying contributions from the *s*-type orbital [note that the size of the black circles in Figs. 2(a)–2(d) is proportional to the contribution projected on the *s*-type orbital]. Our results show that for strain values below 4.6% contribution of the *s*-type orbital is generally confined to the conduction band, which gradually shifts down toward the top of the valence band at the Γ point with increasing strain. At the critical value of 4.6% strain, the valance and conduction bands touch each other and the *s*-type character is acquired by the valence band. When the strain increases beyond 4.6%, the contribution of the *s*-type orbital stays in the valence band, resulting in band inversion at the Γ point.

The observation of band inversion indicates that a topological phase transition occurs with strain. Figs. 2(e)–2(g)

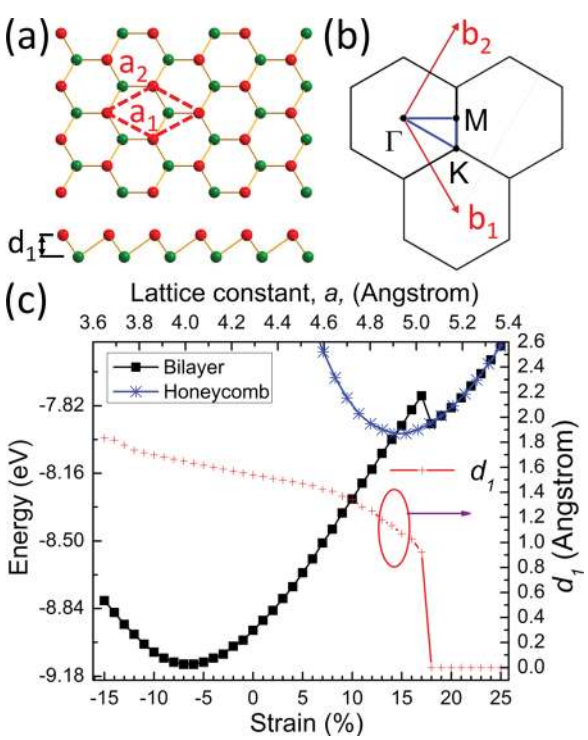

FIG. 1. (a) Side view and top view of crystal structure of Sb single bilayer. (b) 2D Brillouin-zones. Specific symmetry points are labeled. (c) Energies of the single bilayer and planar honeycomb structures as a function of stain (lattice constant). The strain is with respect to the lattice constant of crystalline Sb. The vertical distance, d_1, between two Sb atoms as a function of strain (lattice constant) is also included.

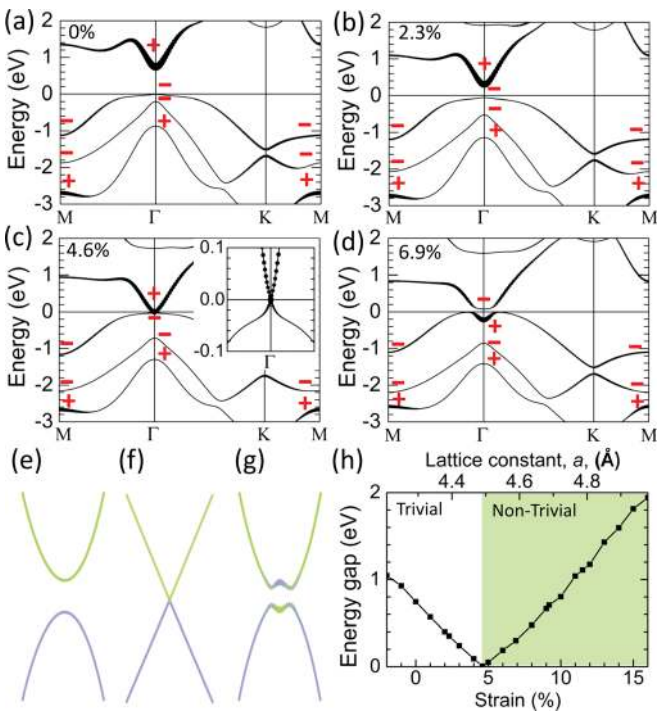

FIG. 2. Band structure of one bilayer Sb under (a) 0%, (b) 2.3%, (c) 4.6%, and (d) 6.9% strain. The inset in (c) is the magnified band near the Γ point. The path in Brillouin zones is M-Γ-K-M. The size of the black circles is proportional to the contributions projected on the *s*-type orbital. The band diagrams are to illustrate (e) the trivial state, (f) the transition point, and (g) the non-trivial state. (h) Plot of band gap as a function of strain (lattice constant) at the Γ point.

illustrate the topological phase transition. The band diagrams are illustrated (e) for the trivial state, (f) at the critical point, and (g) for the nontrivial state. The critical point at zero gap separates two distinct topological phases, see Fig. 2(h). While the trivial side has no band inversion, the nontrivial side shows band inversion where the conduction and valence bands swap their band character at the time reversal invariant point.

So far, we have shown that Sb bilayers under sufficiently large tensile strains are topological insulators with an inverted order of bands. To understand the origin of the band inversion, a scaling factor λ was added artificially in front of the SOC term in the computations. When λ was decreased from 1 to 0, the band gap was closed and reopened. This indicates that the band inversion indeed originates from SOC and is a salient feature of a topological insulator.

In the following, we apply a rigorous method to show that Sb bilayer with a small tensile strain is a topologically trivial band insulator with $Z_2 = 0$, while for larger strains, it is in a nontrivial QSH state with $Z_2 = 1$. We exploit the wave function parity analysis[30] to identify the Z_2 topological phases. This method is valid here since the bilayer structure possesses inversion symmetry. There are four time reversal invariant points in the 2D Brillouin zone for the hexagonal lattice: one is at the Γ point and the other three are at the equivalent M points, see Fig. 1(b). The valence electrons form five bands, and the parity eigenvalues at both Γ and M points are in the order of $-\,+\,+\,-\,-$ from low to high energy for the Sb bilayer with zero strain. Thus, the products of the parity eigenvalues at these two momenta are both -1, yielding a trivial topological invariant $Z_2 = 0$. As the strain is increased beyond 4.6%, band inversion at the Γ point takes place. The parity eigenvalue of the top valence states at the Γ point changes sign to become $+$, while those at the M points remain $-$. Thus, the products of the parity eigenvalues at these two points are now distinct and the Sb bilayers with tensile strains above 4.6% are identified as topological insulators with $Z_2 = 1$.

As the bilayer transforms into the planar honeycomb structure at a strain value of 18%, the valence and conduction bands reshuffle and the parity eigenvalues for the occupied states change. The parity eigenvalues are in the order of $+\,-\,+\,+\,-$ from low to high energy at the Γ point and $-\,+\,-\,+\,+$ at the M points. The products of the parity eigenvalues at these two momenta are both -1, yielding a trivial topological invariant $Z_2 = 0$.

The buckled Sb bilayer naturally provides an advantage in controlling the band gap via an out-of-plane external electric field (gating). The two Sb atoms become inequivalent when the thin film is placed on a substrate or subjected to an external field and the inversion symmetry is removed as illustrated in Fig. 3(a). The spin degeneracy for states away from the high symmetry momenta is lifted due to the effects of SOC and due to the removal of inversion symmetry. Hence, electric field provides a means for producing spin-polarized states and realizing a gating controlled topological phase transition. In Figs. 3(b)–3(d), we show the band structures near the Γ point when an external field is applied to the Sb bilayer under 7% strain. The two conduction bands and the two valence bands near the Fermi level are seen to be

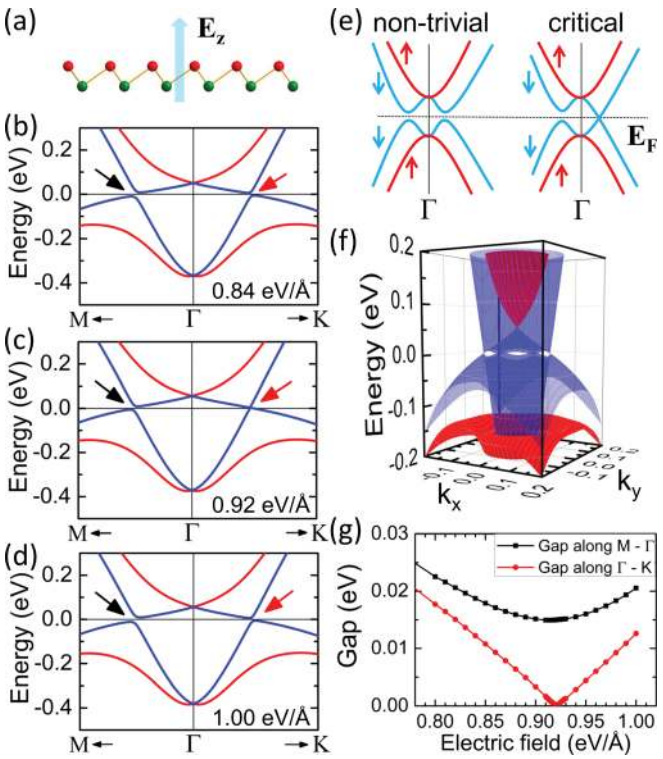

FIG. 3. (a) An Sb single bilayer after adding an out-of-plane E-field. Two different colors are used to identify the two kinds of atoms involved to highlight inversion symmetry breaking. Band structures of one bilayer Sb under out-of-plane electric fields (b) 0.84 V/Å, and (c) 0.92 V/Å, and (d) 1.00 V/Å. The red and blue represent counter-clockwise and clockwise spin helicity, respectively. (e) Topological phase transition due to an out-of-plane electric field. (g) Band gaps along M-Γ and Γ-K, respectively, indicated by black and red arrows in (b) are plotted as a function of the electric field. (f) 3D band dispersions around Γ at 0.92 V/Å.

non-degenerate spin-split states except at the Γ point. By monitoring the band gap size as a function of the strength of the external field in Fig. 3(g), a topological phase transition takes place around 0.92 V/Å where the band gap closes along the $\overline{\Gamma K}$ direction. At the topological critical point, the conduction and valence bands touch at six points, forming six spin-polarized Dirac cones with the Dirac points lying at the Fermi level, as shown in Figs. 3(e) and 3(f).

We further investigated the spin texture of the four states (two below and two above the Fermi level) for the Sb bilayer when the inversion symmetry is broken by an external field. The spin and momentum are one-to-one locked in each band. In Figs. 4(a)–4(d), we show the spin texture for the four bands from the highest to the lowest in energy around the Γ point. The spin helicity is counter-clockwise for the highest [Fig. 4(a)] and the lowest [Fig. 4(d)] bands. The helicity of the two bands in the middle is clockwise as shown in Figs. 4(b) and 4(c). We note that the spin directions of the spin-split states can be reversed by changing the direction of the applied field, i.e., the spin helicities can be flipped by reversing the direction of the external field. The tunability of the spin direction makes the Sb bilayer attractive for spintronic devices.

Concerning the practical realization of topologically nontrivial Sb(111) bilayer, as shown by the shaded region in Fig. 2(h), the non-trivial insulating phase is predicted to exist over the lattice constant window of 4.5 to 4.85 Å. The standard

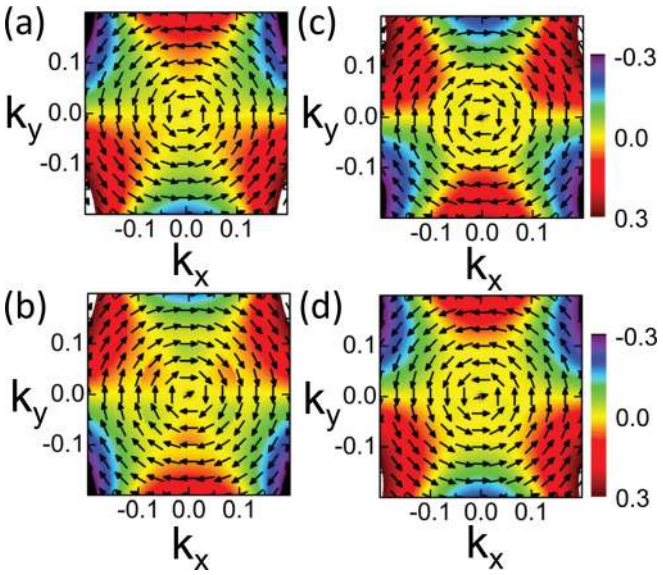

FIG. 4. (a)–(d) are the spin orientations of the four bands (from top to bottom in Fig. 3(f)) projected on k_x and k_y. The out-of-plane spin polarization is color-scaled as the background in the 2D plot.

candidate insulating or semiconducting substrates, such as InSb, Al_2O_3, BC_2N, SiO_2, graphite, diamond, and BN, fall well around the range. It is reasonable therefore to expect that the proper binding can be achieved on an appropriate substrate to generate the non-trivial insulating phase of the Sb(111) bilayer in a (1×1) or a larger unit cell.

To summarize, we have studied the crystal and electronic structures of an Sb single bilayer under strain and investigated the band topologies of the strained bilayer using first-principle calculations with the inclusion of spin-orbit coupling. Nontrivial QSH states can be realized in Sb(111) single bilayer under a tensile strain. The tunability of the spin polarization and the size of the band gap are attractive features for potential applications of Sb thin films in spintronics.

F.C.C. acknowledges support from the National Center for Theoretical Sciences and the Taiwan National Science Council under Grant Nos. NSC-98-2112-M110-002-MY3, and NSC-101-2112-M110-002-MY3. F.C.C. is grateful to the National Center for High-performance Computing for computer time and facilities. The work at Northeastern University was supported by the U.S. Department of Energy, Office of Science, Basic Energy Sciences Contract No. DE-FG02-07ER46352, and benefited from theory support at the Advanced Light Source and the allocation of supercomputer time at NERSC through Grant No. DE-AC02-05CH11231. V.O. was supported as part of "Molecularly Engineered Energy Materials," an Energy Frontier Research Center funded by the U.S. Department of Energy, Office of Science, Basic Energy Sciences under Award No. DE-SC0001342 and used computing resources at NERSC under Contract No. DE-AC02-05CH11231.

[1]J. E. Moore, Nature **464**, 194–198 (2010).
[2]M. Z. Hasan and C. L. Kane, Rev. Mod. Phys. **82**, 3045–3067 (2010).
[3]X.-L. Qi and S.-C. Zhang, Rev. Mod. Phys. **83**, 1057–1110 (2011).
[4]C. L. Kane and E. J. Mele, Phys. Rev. Lett. **95**, 146802 (2005).
[5]B. A. Bernevig and S.-C. Zhang, Phys. Rev. Lett. **96**, 106802 (2006).
[6]C. Xu and J. E. Moore, Phys. Rev. B **73**, 045322 (2006).
[7]D. Hsieh, D. Qian, L. Wray, Y. Xia, Y. S. Hor, R. J. Cava, and M. Z. Hasan, Nature **452**, 970 (2008).
[8]Y. S. Hor, A. Richardella, P. Roushan, Y. Xia, J. G. Checkelsky, A. Yazdani, M. Z. Hasan, N. P. Ong, and R. J. Cava, Phys. Rev. B **79**, 195208 (2009).
[9]D. Hsieh, Y. Xia, D. Qian, L. Wray, J. H. Dil, F. Meier, J. Osterwalder, L. Patthey, J. G. Checkelsky, N. P. Ong, A. V. Fedorov, H. Lin, A. Bansil, D. Grauer, Y. S. Hor, R. J. Cava, and M. Z. Hasan, Nature **460**, 1101 (2009).
[10]S. R. Park, W. S. Jung, C. Kim, D. J. Song, C. Kim, S. Kimura, K. D. Lee, and N. Hur, Phys. Rev. B **81**, 041405R (2010).
[11]Y. L. Chen, J. G. Analytis, J. H. Chu, Z. K. Liu, S. K. Mo, X. L. Qi, H. J. Zhang, D. H. Lu, X. Dai, Z. Fang, S. C. Zhang, I. R. Fisher, Z. Hussain, and Z. X. Shen, Science **325**, 178 (2009).
[12]D. Hsieh, Y. Xia, D. Qian, L. Wray, F. Meier, J. H. Dil, J. Osterwalder, L. Patthey, A. V. Fedorov, H. Lin, A. Bansil, D. Grauer, Y. S. Hor, R. J. Cava, and M. Z. Hasan, Phys. Rev. Lett. **103**, 146401 (2009).
[13]X. Gonze, J.-P. Michenaud and J.-P. Vigneron, Phys. Rev. B **41**, 11827 (1990).
[14]B. A. Bernevig, T. L. Hughes, and S.-C. Zhang, Science **314**, 1757 (2006).
[15]M. Knig, S. Wiedmann, C. Bre, A. Roth, H. Buhmann, L. W. Molenkamp, X.-L. Qi, and S.-C. Zhang, Science **318**, 766 (2007).
[16]A. Roth, C. Brne, H. Buhmann, L. W. Molenkamp, J. Maciejko, X.-L. Qi, and S.-C. Zhang, Science **325**, 294 (2009).
[17]S. Murakami, Phys. Rev. Lett. **97**, 236805 (2006).
[18]M. Wada, S. Murakami, F. Freimuth, and G. Bihlmayer, Phys. Rev. B **83**, 121310 (2011).
[19]H.-Z. Lu, W.-Y. Shan, W. Yao, Q. Niu, and S.-Q. Shen, Phys. Rev. B **81**, 115407 (2010).
[20]C.-X. Liu, H. Zhang, B. Yan, X.-L. Qi, T. Frauenheim, X. Dai, Z. Fang, and S.-C. Zhang, Phys. Rev. B **81**, 041307 (2010).
[21]Z. Liu, C.-X. Liu, Y.-S. Wu, W.-H. Duan, F. Liu, and J. Wu, Phys. Rev. Lett. **107**, 136805 (2011).
[22]G. Bian, T. Miller, and T.-C. Chiang, Phys. Rev. Lett. **107**, 036802 (2011).
[23]P. Zhang, Z. Liu, W. Duan, F. Liu, and J. Wu, Phys. Rev. B **85**, 201410(R) (2012).
[24]P. Hohenberg and W. Kohn, Phys. Rev. **136**, B864 (1964); W. Kohn and L. J. Sham, *ibid.* **140**, A1133 (1965).
[25]D. M. Ceperley and B. J. Alder, Phys. Rev. Lett. **45**, 566 (1980).
[26]J. P. Perdew and A. Zunger, Phys. Rev. B **23**, 5048 (1981).
[27]G. Kresse and D. Joubert, Phys. Rev. B **59**, 1758 (1999).
[28]G. Kresse and J. Hafner, Phys. Rev. B **47**, 558 (1993); G. Kresse and J. Furthmuller, *ibid.* **54**, 11169 (1996).
[29]H. J. Monkhorst and J. D. Pack, Phys. Rev. B **13**, 5188 (1976).
[30]L. Fu and C. L. Kane, Phys. Rev. B **76**, 045302 (2007).